Experimental Verification of Current Ripple Amplitude in Five-Phase PWM VSIs

J. Loncarski [1], O. Dordevic [2], G. Grandi [1]
[1] *Department of Electrical, Electronic and Information Engineering*
Alma Mater Studiorum - University of Bologna, Italy
[2] *Liverpool John Moores University, Liverpool, UK*
jelena.loncarski2@unibo.it, O.Dordevic@ljmu.ac.uk, gabriele.grandi@unibo.it

***Abstract*— Multiphase systems are nowadays considered a viable solution for various industrial applications. Numerous PWM schemes for multiphase voltage source inverters with sinusoidal outputs have been developed, but no detailed analysis of the impact of these modulation schemes on the output peak-to-peak current ripple amplitude has been reported. Determination of the current ripple in multiphase PWM voltage source inverters is interesting from the theoretical point of view and, in some cases, is useful for both design and control purposes. This paper gives the complete analysis of the peak-to-peak current ripple distribution over a fundamental period with experimental verification in the case of five-phase voltage source inverters. In particular, peak-to-peak current ripple amplitude is analytically determined as a function of the modulation index with a symmetrical centered PWM, being the most simple and effective solution to maximize the dc bus utilization, leading to a nearly-optimal modulation to minimize the rms of the current ripple. However, the analysis could be easily extended to either discontinuous or asymmetrical modulation, both carrier-based and space vector PWM.**

Keywords—Output current ripple; multiphase drives; space vector PWM; voltage source inverter; switching sequence.

I. INTRODUCTION

Multiphase motor drives have many advantages over the traditional 3-phase motor drives. Some of them are the ability to reduce the amplitude and increase the frequency of the torque pulsations, to mitigate the rotor harmonic current losses and to reduce the dc link current harmonics. In addition, owing to their redundant structure, multiphase motor drives improve the system reliability [1]-[4].

To overcome the problems related to high-power applications, the increase of the number of phases is considered as a viable solution. In the past decades, multilevel inverter-fed 3-phase ac machines have emerged as a promising solution in achieving high power ratings with voltage limited devices. Similarly, the use of multiphase inverters together with multiphase ac machines has been recognized as a viable approach to obtain high power ratings with current limited devices.

Space vector theory can represent the behavior of the multiphase systems, as a natural extension of the traditional 3-phase space vector transformation, leading to an elegant and effective vectorial approach in multiple α–β planes [5]. Even more, the space vectors can be usefully adopted for the modulation of multiphase inverters. The space vector modulation (SVM) for 5-phase voltage source inverters (VSIs) has been developed in [6]-[9]. In general, for any number of phases, it has been proven that the SV-PWM provides the same switching pattern as the carried-based (CB) PWM, with a proper common-mode injection into the modulating signals [10]. In particular, centering the modulating signals (min-max centering) corresponds to equally share the null vector between the two null configurations.

Recent studies about rms output current ripple in multiphase motor drives are given in [11]-[13], considering a 5-phase system. In [11] the optimal value of the common-mode voltage injection in CB-PWM has been analytically determined to minimize the rms current ripple in each switching period. Furthermore, it is shown that the strategy called SV-PWM, corresponding to centered and symmetric modulation, has a nearly-optimal behavior in terms of the current ripple rms. In [12] it is shown that sinusoidal PWM (SPWM) shows a better performance compared to both 5th harmonic injection PWM (FHIPWM) and SV-PWM but, from the practical point of view, differences in current ripple rms are relatively small considering all these three modulation techniques. In [13] two SV-PWM techniques with 4 large, and 2 large and 2 medium vectors are compared in terms of THD of the current and voltage with established correlations between the flux HDF and the current THD, and squared rms current ripple. In [14] an attempt to evaluate the output rms current ripple has been reported, on the basis of polygon load connection and phase variables in the original domain. However, only a single (adjacent) polygon connection has been used, and the calculated output current-ripple rms does not represent the total output current ripple [15].

In addition to the rms analysis, the benefit of the peak-to-peak current ripple evaluation is recognized in [16], where the ripple amplitude is investigated for 3-phase PWM inverters. A more detailed investigation is presented in [17], providing analytical expressions of a peak-to-peak current ripple distribution over the fundamental period. Simple and effective expressions to determine the maximum and the minimum of the current ripple amplitude in the fundamental period are also given.

From the practical point of view, the knowledge of the peak-to-peak current ripple distribution can be useful to determine the output voltage distortion due to the switch dead-time in case of output currents with high ripple by determining their multiple zero-crossing intervals [18]. The effects of high-ripple currents on dead-time with adaptive compensation are studied in [19] and [20] as well, where the knowledge of peak-to-peak current ripple was of interest but it has not been prop-

erly addressed. Another example of application is referred to hysteresis current controllers and variable switching frequency PWM, for single-phase [21] and three-phase inverters [22], [23]. Furthermore, the peak-to-peak current ripple amplitude, in addition to the fundamental current component, is useful to determine the absolute current peak, affecting the thresholds of protection systems and the design of power components.

The analysis of peak-to-peak output current ripple amplitude is extended also to the cases of 5- and 7-phase VSIs [24], [25]. In [26] the comparison of the peak-to-peak current ripple distribution over a fundamental period for multiphase VSIs is given, starting from 3-phase and extended to the multiphase inverters, with emphasis on 5 and 7 phases. This paper represents an extension of [24], where analysis of the output current ripple is developed for 5-phase PWM inverters. Now the results are experimentally verified for all the relevant cases. The analysis is developed with reference to centered symmetric switching patterns, generated either by CB- or SV-PWM. Detailed analytical expressions of the peak-to-peak current ripple amplitude distribution over a fundamental period are given as a function of the modulation index. The instantaneous current ripple is introduced for a generic balanced inductive load, and the experimental verification is obtained using a passive RL load.

II. Evaluation of Peak-to-Peak Current Ripple Amplitude

A. Multiple space vectors modulation

Multiple space vectors are introduced to represent voltage and current phase quantities in multiphase systems [5]. With reference to a 5-phase VSI supplied by the dc voltage V_{dc}, the output voltage space vectors $\boldsymbol{v_1}$ and $\boldsymbol{v_3}$ can be written as a function of the 5 switching leg states $S_k = [0, 1]$ as

$$\begin{cases} \boldsymbol{v}_1 = \frac{2}{5} V_{dc}\left[S_1 + S_2\boldsymbol{\alpha} + S_3\boldsymbol{\alpha}^2 + S_4\boldsymbol{\alpha}^3 + S_5\boldsymbol{\alpha}^4\right] \\ \boldsymbol{v}_3 = \frac{2}{5} V_{dc}\left[S_1 + S_2\boldsymbol{\alpha}^3 + S_3\boldsymbol{\alpha} + S_4\boldsymbol{\alpha}^4 + S_5\boldsymbol{\alpha}^2\right]. \end{cases} \quad (1)$$

The space vector diagrams representing all possible switch configurations in planes α_1–β_1 and α_3–β_3 are given in Fig. 1.

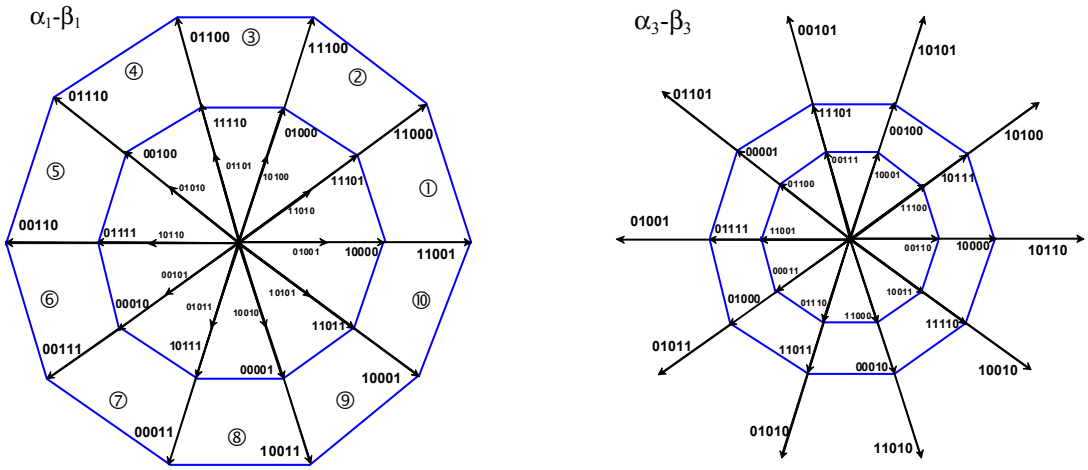

Fig. 1. Space vector diagrams of inverter output voltage in the planes α_1-β_1 and α_3-β_3 .

The SV-PWM of a 5-phase inverter is based on the determination of application times of active and null inverter voltage vectors $\boldsymbol{v}_1$ and $\boldsymbol{v}_3$ in every switching period T_s. In the case of symmetrical SV-PWM, the sequence is determined in $T_s/2$ and it is repeated symmetrically in the next half of the switching period. By equally sharing the application time of the null voltage vector between the switch configurations 00000 and 11111, the so called "centered" switching pattern is realized. In this way, a nearly-optimal modulation able to minimize the rms of current ripple is obtained [11]. As a result of the SV-PWM, the average value of the inverter output voltage $\bar{v}(T_s)$ corresponds to the reference voltage v^*, for each phase.

In the considered case of sinusoidal balanced output voltages supplying a balanced load, the zero-sequence component is null. Introducing the modulation index $m = V^*/V_{dc}$, the reference space voltage vectors become

$$\begin{cases} \boldsymbol{v}_1^* = \boldsymbol{v}^* = m V_{dc} e^{j\vartheta} \\ \boldsymbol{v}_3^* = 0\ . \end{cases} \quad (2)$$

In this case, SV modulation is quarter-wave symmetric, and it can be analyzed in the range $[0, \pi/2]$ of the phase angle $\vartheta = \omega t$. With reference to Fig. 2, the two sectors ① and ② are considered for $0 \le \vartheta \le \pi/5$ and $\pi/5 \le \vartheta \le 2\pi/5$, respectively, and the half of the sector ③ is considered for $2\pi/5 \le \vartheta \le \pi/2$.

For sector ① the application times of the switch configurations involved in the modulation sequence from 00000 to 11111 in the half period $T_s/2$ can be determined as in [6] and [24], and can be extended to any sector k by replacing the phase angle ϑ by ϑ–$(k$–$1)\pi/5$, $k = 1, 2, \ldots, 10$.

Note that the modulation limit is $m \le m_{\max} \approx 0.526$, according to the generalized expression given in [27] for n phases, $m_{\max} = [2 \cos(\pi/2n)]^{-1}$.

B. Ripple evaluation

The alternating voltage component can be written by introducing the averaging over the switching period as in [24]

$$\tilde{v}(t) = v(t) - \bar{v}(T_s), \quad (3)$$

which allows defining the instantaneous current ripple as

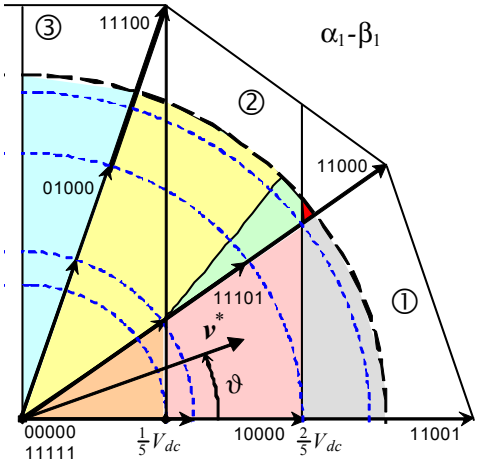

Fig. 2. Space vector diagram of inverter output voltage on plane α_1–β_1 in the range $\vartheta = [0, 90°]$. Outer dashed circle is the modulation limit, $m_{max} \approx 0.526$

$$\tilde{i}(t) = \Delta i(t) - \frac{t}{T_s}\Delta i \cong \frac{1}{L}\int_0^t \tilde{v}(t)dt \,. \tag{4}$$

The peak-to-peak current ripple amplitude is practically the envelope of (4), and it can be calculated as

$$\tilde{i}_{pp} = max\left\{\tilde{i}(t)\right\}_0^{T_s} - min\left\{\tilde{i}(t)\right\}_0^{T_s} \,. \tag{5}$$

Due to the symmetry among all phases in the considered case of sinusoidal balanced currents, only the first phase is examined in the following analysis. For the first phase, the phase quantity results in the projection of the two corresponding space vectors on the real axes. In particular, the average output voltage of the first phase is given by

$$\bar{v}(T_s) = v^* = \Re e\{\boldsymbol{v}_1^*\} + \Re e\{\boldsymbol{v}_3^*\} = mV_{dc}\cos\vartheta \,. \tag{6}$$

By introducing (6) into (3), and calculating $v(t)$ by (1), the alternating component for the first phase of the inverter output voltage can be written as

$$\tilde{v}(t) = \left[S_1 - \frac{1}{5}\left(S_1 + S_2 + S_3 + S_4 + S_5\right)\right]V_{dc} - mV_{dc}\cos\vartheta \,. \tag{7}$$

In order to evaluate the current ripple in the whole phase angle range $0 < \vartheta < \pi/2$, three main cases corresponding to the three sectors depicted in Fig. 2 should be considered. Additional sub-cases determined by the value of modulation index are identified in Fig. 2 with different colors. The complete analysis with further detailed explanations is given in the following sub-sections.

1) Evaluation in the first sector

Considering sector ①, $0 \le \vartheta \le \pi/5$, three different sub-cases can be identified: $0 \le m\cos\vartheta \le 1/5$, $1/5 \le m\cos\vartheta \le 2/5$, and $2/5 \le m\cos\vartheta \le m_{\max}\cos\vartheta < 3/5$. These three sub-cases are represented in Fig. 3.

The sub-case $0 \le m\cos\vartheta \le 1/5$ (orange area in Fig. 2) is considered in diagram ❶ of Fig. 3, where the current ripple $\tilde{i}$ and its peak-to-peak value $\tilde{i}_{pp}$ are depicted, together with the instantaneous output voltage $v(t)$. In this case, according to Fig. 3, $\tilde{i}_{pp}$ can be evaluated by (4), (5) and (7), considering the switch configurations 11111 or 00000 with the corresponding application interval t_0, leading to

$$\tilde{i}_{pp} = \frac{1}{L}\left\{mV_{dc}\cos\vartheta\, t_0\right\}. \tag{8}$$

The sub-case $1/5 \le m\cos\vartheta \le 2/5$ (pink area in Fig. 2) is depicted in diagram ❷ of Fig. 3. In this case $\tilde{i}_{pp}$ can be evaluated considering the switch configurations 11111 and 11101, with corresponding application intervals $t_0/2$ and t_4, leading to

$$\tilde{i}_{pp} = \frac{2}{L}\left\{mV_{dc}\cos\vartheta\frac{t_0}{2} + \left(mV_{dc}\cos\vartheta - \frac{V_{dc}}{5}\right)t_4\right\}. \tag{9}$$

The sub-case $2/5 \le m\cos\vartheta \le m_{\max}\cos\vartheta$ (gray area in Fig. 2) is depicted in diagram ❸ of Fig. 3. In this case $\tilde{i}_{pp}$ can be evaluated considering the switch configurations 11111, 11101, and 11001, with the corresponding application intervals $t_0/2$, t_4, and t_3, leading to

$$\tilde{i}_{pp} = \frac{2}{L}\left\{mV_{dc}\cos\vartheta\frac{t_0}{2} + \left(mV_{dc}\cos\vartheta - \frac{V_{dc}}{5}\right)t_4 + \left(mV_{dc}\cos\vartheta - \frac{2V_{dc}}{5}\right)t_3\right\}. \tag{10}$$

2) Evaluation in the second sector

Considering sector ②, $\pi/5 \le \vartheta \le 2\pi/5$, three different sub-cases can be identified: $0 \le m\cos\vartheta \le 1/5$, $1/5 \le m\cos\vartheta \le 2/5$, and $2/5 \le m\cos\vartheta \le m_{\max}\cos\vartheta < 3/5$. These three sub-cases are represented in Fig. 4.

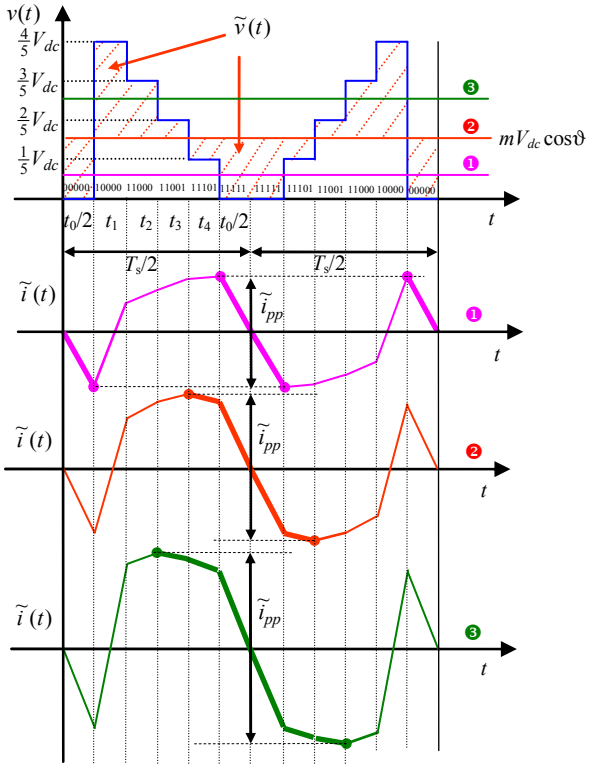

Fig. 3. Output voltage and current ripple in one switching period for sector ①, $0 \le \vartheta \le \pi/5$.

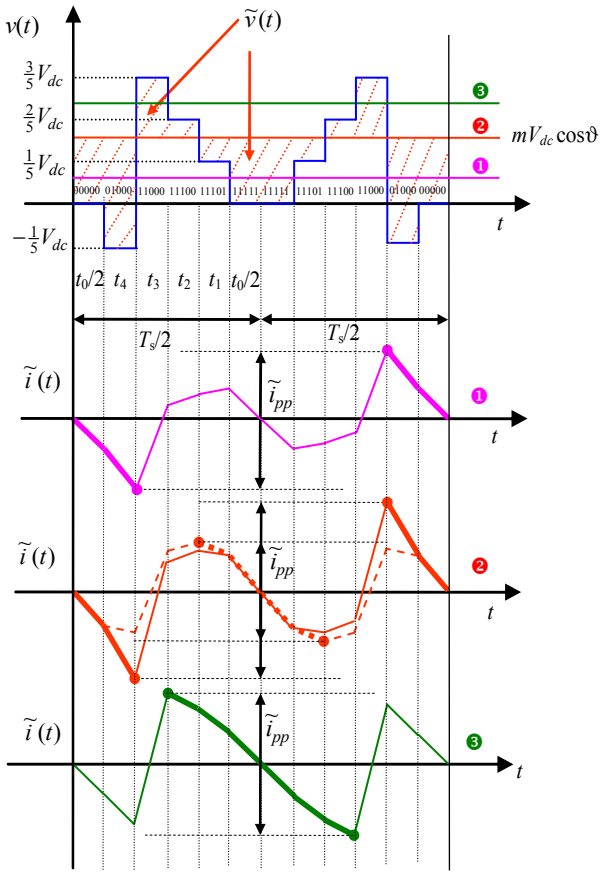

Fig. 4. Output voltage and current ripple in one switching period for sector ②, $\pi/5 \le \vartheta \le 2\pi/5$.

It can be noticed that in the second sub-case there are two possible situations for the evaluation of $\tilde{i}_{pp}$, corresponding to the yellow-green areas of sector ② in Fig. 2.

The sub-case $0 \le m\cos\vartheta \le 1/5$ (yellow area in Fig. 2) is depicted in diagram ❶ of Fig. 4. According to this figure, $\tilde{i}_{pp}$ can be evaluated by (4), (5), and (7), considering the switch configurations 00000 and 01000 with corresponding application intervals $t_0/2$ and t_4

$$\tilde{i}_{pp} = \frac{2}{L}\left\{ mV_{dc}\cos\vartheta\,\frac{t_0}{2} + \left(mV_{dc}\cos\vartheta + \frac{1}{5}V_{dc} \right) t_4 \right\}. \qquad (11)$$

The sub-case $1/5 \le m\cos\vartheta \le 2/5$ is depicted in diagram ❷ of Fig. 4. According to this figure, two different situations are possible, and the resulting $\tilde{i}_{pp}$ is the greater one:

- in the first situation, yellow area, (solid orange line in Fig. 4), $\tilde{i}_{pp}$ can be determined as in the previous sub-case by considering the switch configurations 00000 and 01000 with the application intervals $t_0/2$ and t_4, leading to (11);
- in the second situation, green area, (dashed orange line in Fig. 4), $\tilde{i}_{pp}$ can be determined by considering the switch configurations 11111 and 11101 with the corresponding application intervals $t_0/2$ and t_1, leading to

$$\tilde{i}_{pp} = \frac{2}{L}\left\{ mV_{dc}\cos\vartheta\,\frac{t_0}{2} + \left(mV_{dc}\cos\vartheta - \frac{1}{5}V_{dc} \right) t_1 \right\}. \qquad (12)$$

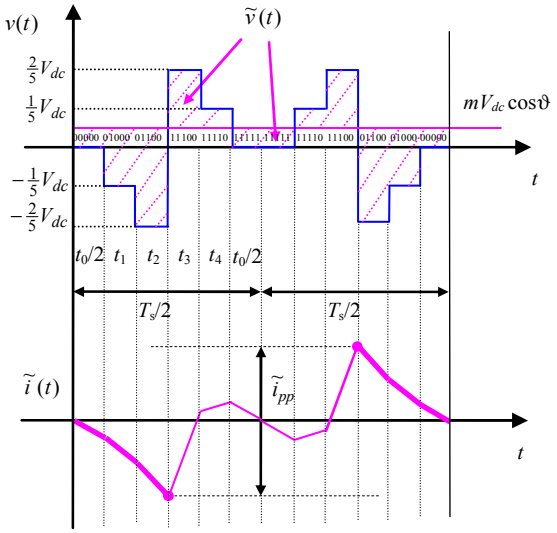

Fig. 5. Output voltage and current ripple in one switching period for sector ③, $2\pi/5 \le \vartheta \le \pi/2$.

The last sub-case $2/5 \le m\cos\vartheta \le m_{\max}\cos\vartheta$ (red area in Fig. 2) is depicted in diagram ❸ of Fig. 4. According to this figure, $\tilde{i}_{pp}$ can be evaluated considering the switch configurations 11111, 11101, and 11100, with the corresponding application intervals $t_0/2$, t_1, and t_2, leading to

$$\tilde{i}_{pp} = \frac{2}{L}\left\{ mV_{dc}\cos\vartheta\,\frac{t_0}{2} + \left(mV_{dc}\cos\vartheta - \frac{V_{dc}}{5} \right) t_1 + \left(mV_{dc}\cos\vartheta - \frac{2V_{dc}}{5} \right) t_2 \right\}. \qquad (13)$$

3) Evaluation in the third sector (half)

With reference to the half of sector ③, $2\pi/5 \le \vartheta \le \pi/2$ (blue area in Fig. 2), there are not sub-cases, and the only occurrence is $0 \le m\cos\vartheta \le m_{\max}\cos\vartheta < 1/5$, as depicted in Fig. 5. In this case, $\tilde{i}_{pp}$ can be evaluated by (4), (5), and (7), considering the switch configurations 00000, 01000, and 01100, with the corresponding application intervals $t_0/2$, t_1, and t_2, as

$$\tilde{i}_{pp} = \frac{2}{L}\left\{ mV_{dc}\cos\vartheta\,\frac{t_0}{2} + \left(mV_{dc}\cos\vartheta + \frac{1}{5}V_{dc} \right) t_1 + \left(mV_{dc}\cos\vartheta + \frac{2}{5}V_{dc} \right) t_2 \right\}. \qquad (14)$$

III. Experimental Results

In order to verify the analytical developments shown in the previous section, experimental tests have been carried out. The experimental setup with custom-built 2-level multiphase inverter is shown in Fig. 6. The load parameters are: R = 22 Ω and L = 8 mH. The dc-bus voltage (V_{dc}) is set to 100 V by Sorensen SGI 600/25 dc supply. The inverter switching frequency ($1/T_s$) is set to 2 kHz, with a dead-time of 6 µs. For the real-time implementation of the code, dSpace ds1006 hardware has been used. The 5-phase system is well balanced and the first phase is selected for further analysis, as in analytical developments. Different values of m have been investigated (0.2, 0.247, 0.4, and 0.494), to cover all the possible cases.

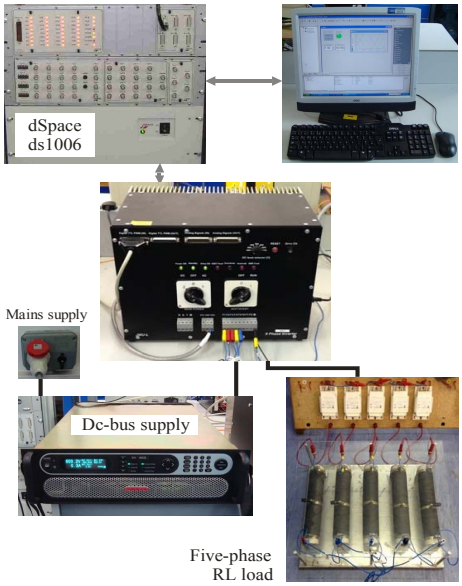

Fig. 6. Experimental setup

One fundamental period of the phase current, for modulation index of $m = 0.2$, is shown in Fig. 7(a). The current $i(t)$ is shown with its fundamental component $i_1(t)$, which was calculated offline in order to extract the current ripple, as $i(t)$-$i_1(t)$. It has been noticed in the results that the ripple was with high 3rd harmonic which was the consequence of the inverter dead-time (5-th harmonic is missing and other odd harmonics were negligible [28]). In order to get experimental results that could be compared with the analytical results presented in Section II, the 3rd harmonic was also subtracted from the output current, leading to the current ripple shown in Fig. 7(b).

In Figs. 8, 9, 10, and 11 is shown the current ripple obtained with experiments (pink color), processed as explained above and also filtered to eliminate the high order harmonics (cut-off frequency 25 kHz). Comparison is made with the half of the peak-to-peak current ripple, $\tilde{i}_{pp}/2$. Positive and negative envelope (blue traces) are determined by the equations presented in Section II.B for the different regions.

The values of the modulation index have been chosen to cover all possible sub-cases (different colored regions in Fig. 2). The agreement is good in the whole fundamental period, proving the effectiveness of the analytical developments.

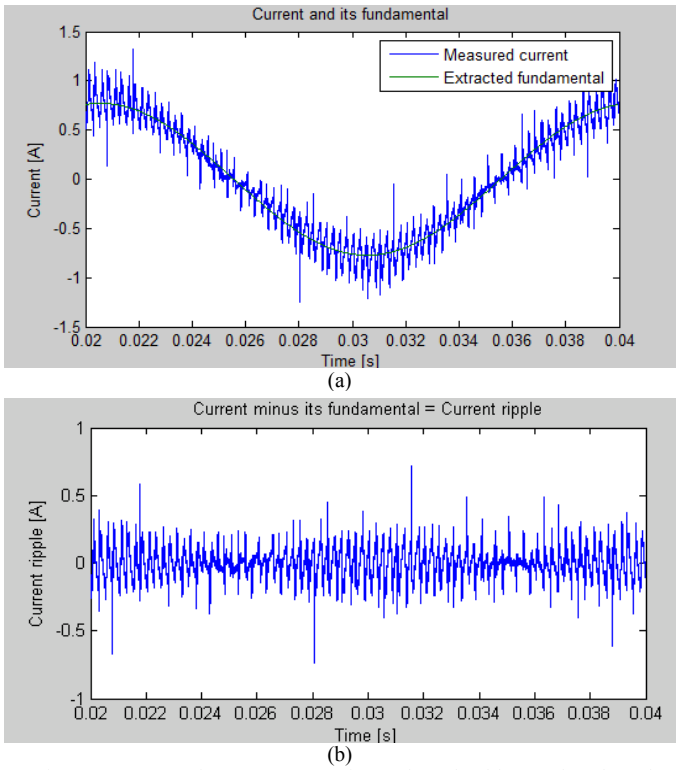

Fig. 7. (a) Current for $m = 0.2$: experimental results (blue) and evaluated fundamental (green), (b) current ripple.

IV. Conclusion

In this paper the peak-to-peak output current ripple in multiphase PWM inverters has been analyzed and experimentally verified with reference to 5-phase VSI. In particular, analytical expressions of the peak-to-peak current ripple amplitude have been developed as a function of the modulation index in the whole fundamental period. All the relevant cases identified by theory have been experimentally verified.

Although the proposed analysis is based on centered symmetrical PWM, it can be easily extended to either discontinuous or asymmetrical modulation, both carrier-based and space vector PWM. Furthermore, the derived analytical expressions can be utilized to minimize the current ripple amplitude by properly adjusting the switching frequency and/or the sharing of the null-voltage-vector application time between the two null switch configurations.

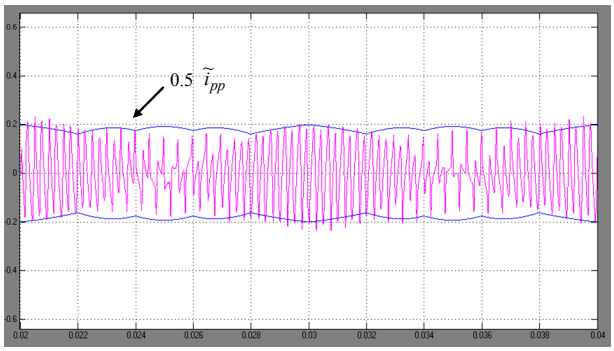

Fig. 8. Current ripple for $m = 0.2$: experimental results (pink) and evaluated peak-to-peak amplitude (blue envelopes) for one fundamental period.

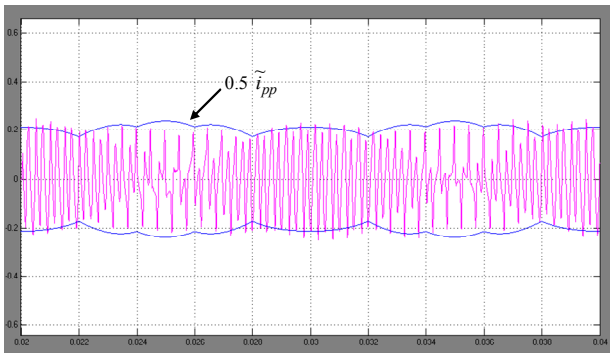

Fig. 9. Current ripple for $m = 0.247$: experimental results (pink) and evaluated peak-to-peak amplitude (blue envelopes) for one fundamental period.

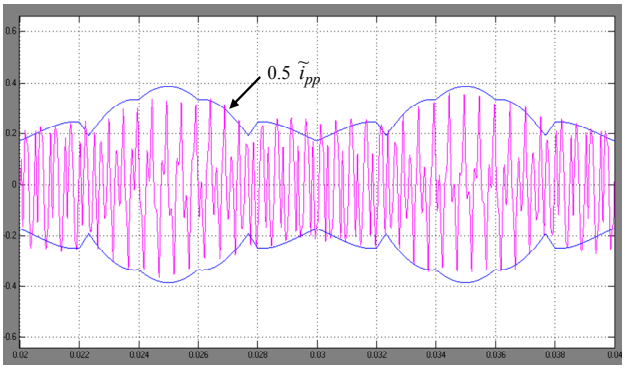

Fig. 10. Current ripple for m = 0.4: experimental results (pink) and evaluated peak-to-peak amplitude (blue envelopes) for one fundamental period.

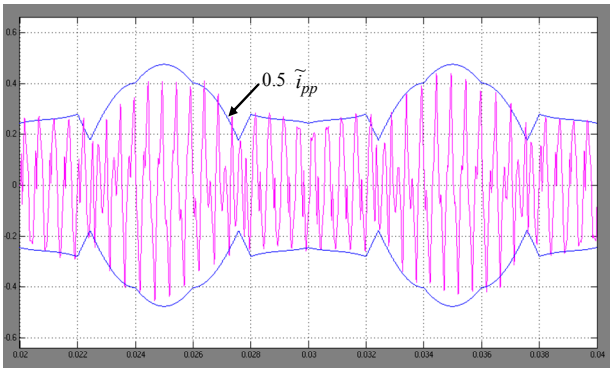

Fig. 11. Current ripple for m = 0.494: experimental results (pink) and evaluated peak-to-peak amplitude (blue envelopes) for one fundamental period.

REFERENCES

[1] H.A. Toliyat, S.P. Waikar, T.A. Lipo, "Analysis and simulation of five-phase synchronous reluctance machines including third harmonic of air-gap MMF," *IEEE Trans. on Industry Applications*, vol. 34, no. 2, pp. 332–339, March/April 1998.

[2] H. Xu, H.A. Toliyat, L.J. Petersen, "Five-phase induction motor drives with DSP-based control system," *IEEE Trans. on Power Electronics*, vol. 17, no. 4, pp. 524–533, July 2002.

[3] H.M. Ryu, J.K. Kim, S.K. Sul, "Synchronous frame current control of multi-phase synchronous motor. Part I. Modelling and current control based on multiple d-q spaces concept under balanced condition," *Proc. of 39th IAS Annual Meeting*, vol. 1, pp. 56–63, 3–7 October 2004.

[4] L. Parsa, H.A. Toliyat, "Five-phase permanent-magnet motor drives," *IEEE Trans. on Industry Applications*, vol. 41, no. 1, pp. 30–37, Jan./Febr. 2005.

[5] G. Grandi, G. Serra, A. Tani, "General analysis of multi-phase systems based on space vector approach," *Proc. of 12th Power Electronics and Motion Control Conference* (*EPE-PEMC*), Portoroz (Slovenia), Aug. 30–Sept. 1, 2006.

[6] H.M. Ryu, J.W. Kim, S.K. Sul, "Analysis of multi-phase space vector pulse width modulation based on multiple d-q spaces concept," *IEEE Trans. on Power Electronics*, vol. 20, no. 6, pp. 1364–1371, Nov. 2005.

[7] A. Iqbal, E. Levi, "Space vector modulation schemes for a five-phase voltage source inverter," *Proc. of European Power Electronic Conference* (*EPE*), Dresden (D), pp. 1–12, Sept. 11–14, 2005.

[8] P.S.N. de Silva, J.E. Fletcher, B.W. Williams, "Development of space vector modulation strategies for five phase voltage source inverters," *Proc. of Power Electronics, Machines and Drives Conference* (*PEMD*), vol. 2, pp. 650–655, March 31–April 2, 2004.

[9] O. Ojo, G. Dong, "Generalized discontinuous carrier-based PWM modulation scheme for multi-phase converter-machine systems," *Proc. of 40th Annual Meeting, IEEE Industry Applications Society*, Hong Kong, pp. 1374–1381, Oct. 2–6, 2005.

[10] A. Iqbal and S. Moinuddin, "Comprehensive relationship between carrier-based PWM and space vector PWM in a five-phase VSI,", *IEEE Trans. On Power Electronics*, vol. 24, no. 10 , pp. 2379–2390, 2009.

[11] D. Casadei, M. Mengoni, G. Serra, A. Tani, L. Zarri "A new carrier-based PWM strategy with minimum output current ripple for five-phase inverters," *Proc. of 14th European Conference on Power Electronics and Application* (*EPE*), pp. 1–10, Aug. 30–Sept. 1 2011.

[12] D. Dujic, M. Jones, E. Levi, "Analysis of output current ripple rms in multiphase drives using space vector approach," *IEEE Trans. On Power Electronics*, vol. 24, no. 8, pp. 1926–1938, August 2009.

[13] M. Jones, D. Dujic, E. Levi, J. Prieto, F. Barrero, "Switching ripple characteristics of space vector PWM schemes for five-phase two-level voltage source inverters-Part2: Current ripple," *IEEE Trans. On Industrial Electronics*, vol. 58, no. 7, pp. 2799–2808, July 2011.

[14] P.A. Dahono, Deni, E.G. Supriatna,"Output current-ripple analysis of five-phase PWM inverters," *IEEE Trans. on Industry Applications*, vol. 45, no. 6, pp. 2022–2029, November/December 2009.

[15] Dujic, M. Jones, E. Levi, "Analysis of output current-ripple RMS in multiphase drives using polygon approach," *IEEE Trans. on Power Electronics*, vol. 25, no. 7, pp. 1838–1849, July 2010.

[16] D. Jiang, F. (Fred) Wang, "Study of analytical current ripple of three-phase PWM converter," *Proc. of 27th IEEE Applied Power Electronics Conference and Exposition* (*APEC*), pp. 1568–1575, 5–9 Feb. 2012.

[17] G. Grandi, J. Loncarski "Evaluation of current ripple amplitude in three-phase PWM voltage source inverters, " *Proc. of 8th International Conference-Workshop Compatibility and Power Electronics* (*CPE*), 5–7 June 2013.

[18] G. Grandi, J. Loncarski, R. Seebacher, "Effects of current ripple on dead-time distortion in three-phase voltage source inverters," *Proc. of 2nd IEEE ENERGYCON Conference & Exhibition - Advances in Energy Conversion*, Florence, Italy, 9–12 Sept. 2012.

[19] M.A. Herran, J.R. Fischer, S.A. Gonzalez, M.G. Judewicz, , D.O. Carrica, "Adaptive dead-time compensation for grid-connected PWM inverters of single-stage PV systems," *IEEE Transaction on Power Electronics*, vol.28, no.6, pp. 2816–2825, June 2013.

[20] J. Schellekens, R. Bierbooms, and J. Duarte, "Dead-time compensation for PWM amplifiers using simple feed-forward techniques," *Proc. of XIX Int. Conference on Electrical Machines* (*ICEM*), pp. 1–6, Sept. 2010.

[21] X. Mao, R. Ayyanar, H. K. Krishnamurthy, "Optimal variable switching frequency scheme for reducing switching loss in single-phase inverters based on time-domain ripple analysis," *IEEE Trans. on Power Electronics*, vol. 24, no. 4, pp. 991–1001, April 2009.

[22] C. Ngai-Man Ho, V.S.P. Cheung, H. Shu-Hung Chung, "Constant-frequency hysteresis current control of grid-connected VSI without bandwidth control," *IEEE Trans. on Power Electronics*, vol. 24, no. 11, pp. 2484–2495, Nov. 2009.

[23] D.G. Holmes, R. Davoodnezhad, B.P. McGrath, "An improved three-phase variable-band hysteresis current regulator," *IEEE Trans. on Power Electronics*, vol. 28, no. 1, pp. 441–450, Jan. 2013.

[24] G. Grandi and J. Loncarski, "Evaluation of current ripple amplitude in five-phase PWM voltage source inverters," *Proc. of IEEE Conference on ICT, Power engineering, and Signal processing* (*EUROCON*), Zagreb (CRO), 1–4 July 2013.

[25] G. Grandi and J. Loncarski, "Analysis of Peak-to-Peak Current Ripple Amplitude in Seven-Phase PWM Voltage Source Inverters", *Energies*, vol. 6, ISSN 1996–1073, 2013.

[26] G. Grandi, J. Loncarski, C. Rossi, "Comparison of Peak-To-Peak Current Ripple Amplitude in Multiphase PWM Voltage Source Inverters," *Proc. of 15th European Conf. on Power Electronics and Applications* (*EPE*), 3–5 Sept 2013.

[27] E. Levi, D. Dujic, M. Jones, G. Grandi, "Analytical determination of DC-bus utilization limits in multi-phase VSI supplied AC drives," *IEEE Trans. on Energy Convers*, vol. 23, no. 2, pp. 433–443, June 2008.

[28] G. Grandi and J. Loncarski, "Analysis of dead-time effects in multi-phase voltage sourse inverters," *Proc. IET Power Electronics, Machines and Drives* (*PEMD*), Bristol, UK, CD-ROM paper 0223, 2012.